A FINITE ELEMENT STUDY ON THE EFFECTS OF TOUGHNESS AND PERMANENT OUT-OF-PLANE DEFORMATION ON POST-IMPACT COMPRESSIVE STRENGTH

D. J. Bull[1], S. M. Spearing[1] and I. Sinclair[1]

[1]Faculty of Engineering and the Environment, University of Southampton,
Southampton, SO17 1BJ, United Kingdom
Email: daniel.bull@soton.ac.uk, web page: southampton.ac.uk/engineering

Keywords: Compression after impact, Finite element modelling, Buckling, Toughness, VCCT

ABSTRACT

This study uses observations of mechanisms from previous work (the "undamaged cone", toughness and extent of permanent out-of-plane deformation) to examine parametrically their effects on residual compression after impact (CAI) strength using finite element models. In previous experimental work, tougher material systems exhibited up to 30% greater CAI strength for a given damage area. Based on this, it is desirable to understand what other parameters, beyond damage area, contribute to the CAI strength. Finite element models were implemented in ABAQUS™ explicit. Delamination growth was modelled using the virtual crack closure technique (VCCT). This study found that systems containing an undamaged cone exhibited an increased load prior to buckling, resulting in lower 0° peak compressive stresses and lower strain energy release rates forming at the outer edges of the delamination zone. In certain configurations, delamination growth into the undamaged cone occurred and was shown to affect negatively the post-buckled response. Overall, the effects of both toughness and permanent out-of-plane deformation was shown to affect CAI failure load by up to ~50% for a given damage diameter. It is also apparent that toughness played a more significant influence than the extent of permanent out-of-plane deformation.

1 INTRODUCTION

Carbon fibre reinforced polymers (CFRPs) are widely reported to be susceptible to low velocity impact damage. This damage directly contributes to a loss in residual compression-after-impact (CAI) strength. Many experimental studies report a correlation with a reduction to CAI strength with an increase in damage area and, therefore, conclude that delaminations are predominantly responsible [1-6].

The sequence of events leading to compressive failure is heavily debated in the literature. Whilst most studies report that local buckling results in a rapid growth of delaminations extending laterally, leading to a sudden loss of load carrying capability [7, 8], other studies report a load redistribution resulting in compressive fibre fracture [9, 10].

There are many CAI modelling studies conducted in the literature. To maintain a simplistic model, many studies consolidate the complex network of delaminations into simplified circular or elliptical delaminations [11]. Models can be purely elastic [12] or can include delamination growth, typically through use of cohesive zone modelling [11, 13]. More complex models have been constructed to include realistic damage patterns and parametrically compare different damage shapes to CAI failure load [12, 14]. Whilst it is important to predict accurately CAI failure, simplifications are usually necessary to enable a reasonable solution time. To ensure accuracy in the model, it is therefore, important to include the key mechanisms that contribute towards CAI failure, and therefore there is a need to make comparisons with experimental findings for verification [15].

In previous experimental work carried out by the authors [16], the role of the "undamaged cone" was shown to play an important effect. In this study, micro-focus computed tomography (μCT) was used to scan impacted coupons, followed by scans taken from interrupted CAI tests immediately prior to failure. This work observed delamination growth through the undamaged cone immediately prior to CAI failure in an untoughened system. This damage growth connected the surrounding delaminations through the undamaged cone thereby destabilising the sublaminates. In particle toughened systems, only partial delamination growth into the undamaged cone was captured and observed. It was noted that no delamination growth was detected extending beyond the damage area prior to CAI failure; however growth associated with pre-existing 0° fibre fracture was observed. Due to the catastrophic and sudden nature of CAI failure, it was inconclusive whether or not rapid delamination growth extending beyond the damage area was the cause of CAI failure.

Another observation made in previous work [16] was the extent of permanent out-of-plane deformation. The indent caused by the local contact of the impact tup was of a greater magnitude (up to 0.3 mm) in toughened systems compared to the untoughened system (~0.15 mm) under 30 J impact and is attributed to local plastic deformation at the impact site. The out-of-plane deformation was shown to affect all the plies through the coupon thickness.

Experimental results from failure load against the size of the damage area revealed that toughened systems exhibited up to 30% more retention of CAI strength compared to untoughened systems for a given damage area. It was therefore, concluded that other parameters such as the extent of out-of-plane deformation, role of the undamaged cone, and toughness can influence residual CAI strength beyond the size of the damage area. Through use of finite element models, this work aims to understand better the contribution of these parameters towards the loss of CAI strength and also aims to understand which failure mechanism (rapid delamination growth or 0° compressive fibre fracture), contributes towards catastrophic CAI failure.

2 METHODOLOGY

2.1 Model setup

The finite element model was conducted using ABAQUS 6.13 explicit software. The model utilises a standard ASTM D7137 test coupon geometry and boundary conditions. This comprised of a test coupon size of 150 x 100 x 4.8 mm using 24 plies and a $[45/0/-45/90]_{3S}$ stacking sequence. An IM7/8551-7 unidirectional carbon fibre system is modelled; the elastic properties are shown in Table 1. To provide parametric variations of interlaminar toughness, five toughness groups were chosen ranging from systems with very low to high toughnesses as shown in Table 2. A Benzeggagh-Kenane mixed-mode failure criterion [17] was used with μ=1. The material has a peak 0° compressive strength (Xc) of 1.6 GPa.

Property		Value
E_{11}	[GPa]	165
E_{22}	[GPa]	8.4
E33	[GPa]	8.4
G12	[GPa]	5.4
G13	[GPa]	5.4
G23	[GPa]	2.8
ν_{12}	–	0.34
ν_{13}	–	0.34
ν_{23}	–	0.5

Table 1: Material elastic properties.

Toughness	Mode I (J/m^2)	Mode II (J/m^2)	Mode III (J/m^2)
V-low	270	600	600
Low	394	875	875
Medium	765	1700	1700
High	1170	2600	2600

Table 2: Material interlaminar toughness properties.

To form the ply stacking sequence in the model, six stacked sublaminates each comprising four plies, were constructed from 4-noded doubly curved general-purpose shell elements with reduced integration (S4R). The sublaminates were assembled using tie constraints enabling pairs of surfaces between sublaminates to be joined together. Delaminations were included between sublaminate pairs and were formed of a simplistic circular shape. The shape was chosen to consolidate the "spiral staircase" delamination pattern into a single circular delamination to minimize the complexity and solution time of the model. Delaminations between pairs of sublaminates were formed of untied regions and used contact constraints to prevent surface penetration. The contact surface encompassed a frictionless and hard contact property. To model delamination growth, virtual crack closure technique (VCCT) elements were included over the undamaged cone region and along the perimeter surrounding the outer delaminated region. To enable local buckling in the model, an imperfection was added to the centre of the sublaminates by displacing the respective nodes out-of-plane. The imperfection followed a "domed" shape with a curvature matching the radius observed in experimental work and was applied to all the sublaminates. The peak depth of the imperfection ranged from 0.02 to 0.4 mm.

A mesh sensitivity study was conducted to offer the best compromise between solution time and accuracy. A fine mesh size with minimum element size of 0.5 mm was chosen within the delamination area and 10 mm outside the delamination perimeter. Mesh refinement was used towards the delamination edges, both towards the undamaged cone and towards the outer perimeter.

Boundary conditions were set to replicate the constraints outlined in the ASTM D7137 CAI tests. To enable displacement control loading of the samples, an in-plane compressive edge displacement of 1 mm was applied to the top edges of the shells to occur over half a second duration. The displacements were applied using the ABAQUS option DEFINITION = SMOOTH to apply the displacements smoothly, and to prevent oscillations to the kinetic energy of the system.

To enable a reasonable solve time with the ABAQUS explicit solver, a time step of 73 ns was used with fixed mass scaling. To ensure confidence in the results, the kinetic energy for each test was monitored and remained two orders of magnitude below the recommended 10% of total internal energy (ABAQUS 6.13 user's manual). Models were solved on the University of Southampton Iridis 4 supercomputer cluster. Each model was solved using 64 cores over 4 nodes with a solution time of between 30 and 34 hours.

Failure was defined in this study when the 0° compressive stress exceeded the critical 0° compressive strength of 1.6 GPa or when delamination growth on the outer delamination perimeter occurred.

2.2 Parametric study

To form a complete parametric study, different combinations of the parameters shown in table 3 were used. In total, 60 models were created, solved and analysed.

Damage diameter (mm)	Toughness	Permanent out-of-plane deformation (mm)	Undamaged cone
20	V-low	0.02	No undamaged cone
30	Low	0.04	With undamaged cone
40	Medium	0.1	
	High	0.4	

Table 3: Model parameters used in this study.

3 RESULTS

3.1 CAI failure mechanisms

There are two routes to loss in load carrying capability from CAI as reported earlier in the introduction. This consists of a load redistribution resulting in compressive fibre fracture or a sudden growth of delaminations extending laterally outwards. The finite element models in this study captured both characteristics as shown in Fig 1 and Fig 2 and are a consequence of the local buckling in the delaminated region. In the post-buckled regime, a compressive stress concentration formed at the outer edges of the delamination perimeter (Fig 1 (i)). These stresses can exceed the Xc critical compressive strength of the 0° ply leading to a loss of local load carrying capability. Alternatively, post-buckling can lead to delamination propagation. In the example shown in Fig 2, delamination growth is observed propagating into the undamaged cone (iii) followed by rapid delamination growth extending laterally outwards (iv). The mode of failure is specific to the damage area, toughness and extent of permanent out-of-plane deformation.

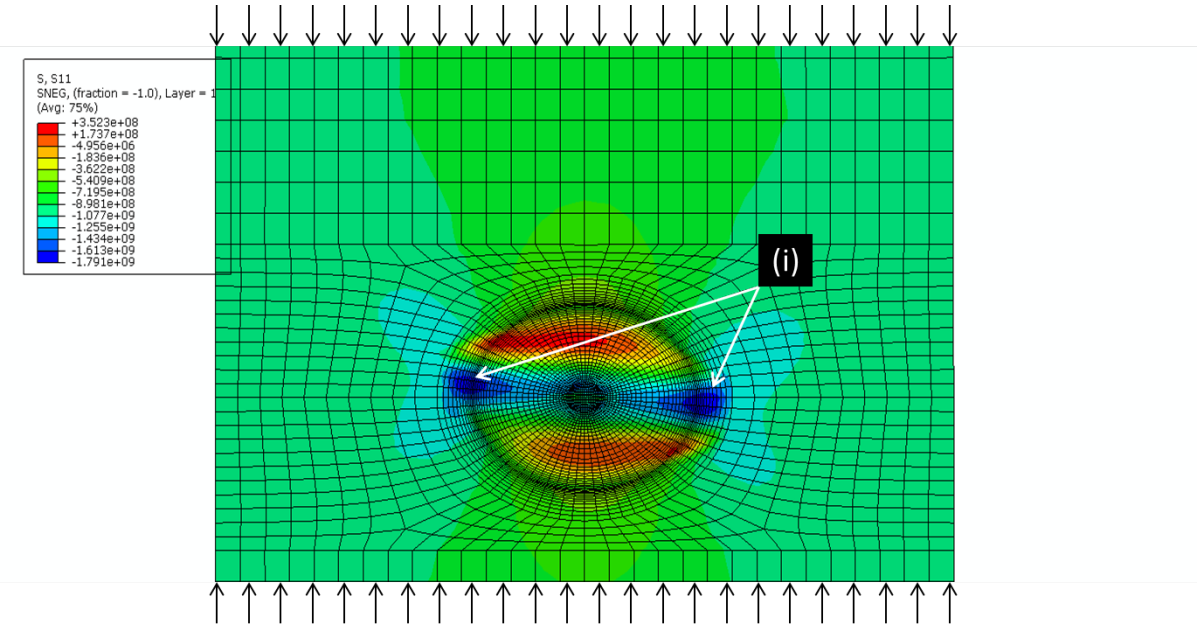

Figure 1: FE model showing 0° in-plane compressive stresses. (i) local 0° ply compressive stress concentration at outer edges of delamination in the post-buckled regime.

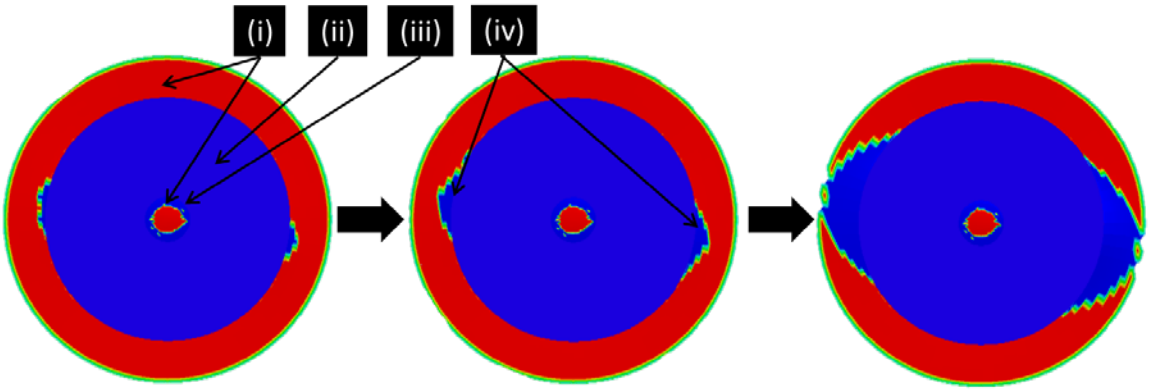

Figure 2: Delamination growth captured at VCCT regions. (i) VCCT regions at the undamaged cone and surrounding the delamination perimeter. (ii) Delamination area. (iii) Undamaged cone with partial delamination growth into this region. (iv) Rapid delamination growth extending laterally at the delamination edges.

3.3 Effect of the undamaged cone

The role of the undamaged cone has been tested to check for significant differences between systems that do not include this feature. Fig 3 shows the effects of the undamaged cone on buckling and post-buckling response at 20, 30, and 40 mm delamination diameters. It is clear that systems containing the undamaged cone result in a reduction in out-of-plane displacement for a given load. This difference was shown to be up to ~50% and was consistent at all damage diameters and all permanent out-of-plane deformations tested.

Fig 4 shows how the inclusion of the undamaged cone affects the three modes of peak strain energy release rate measured at the outer perimeter of the delamination area. The undamaged cone is shown to reduce the peak strain energy release rates under mode I and mode III and in the most part of mode II. Fig 3 also shows the mix mode behaviour with a dominance of mode II and mode III.

Fig 5 highlights the importance of the undamaged cone on the peak 0° compressive stress. Again we see the presence of the undamaged cone results in a greater load carrying capability for a given compressive stress. At the point where the critical Xc stress is reached at 1.6 GPa, there is a 30% difference in the total applied load.

There is a particular link between the out-of-plane displacement (Fig 2) and increase in strain energy release rate (Fig 3) and peak compressive stress (Fig 4). During the post-buckled regime where the rate of out-of-plane displacement increases, there is a corresponding accelerated increase in peak strain energy release rate and 0° compressive stress. It is therefore, clear that a reduction in the out-of-plane displacement due to the undamaged cone is shown to result in a reduction (in the most cases) in peak strain energy release rate (fig 3) and peak 0° compressive stress (fig 4).

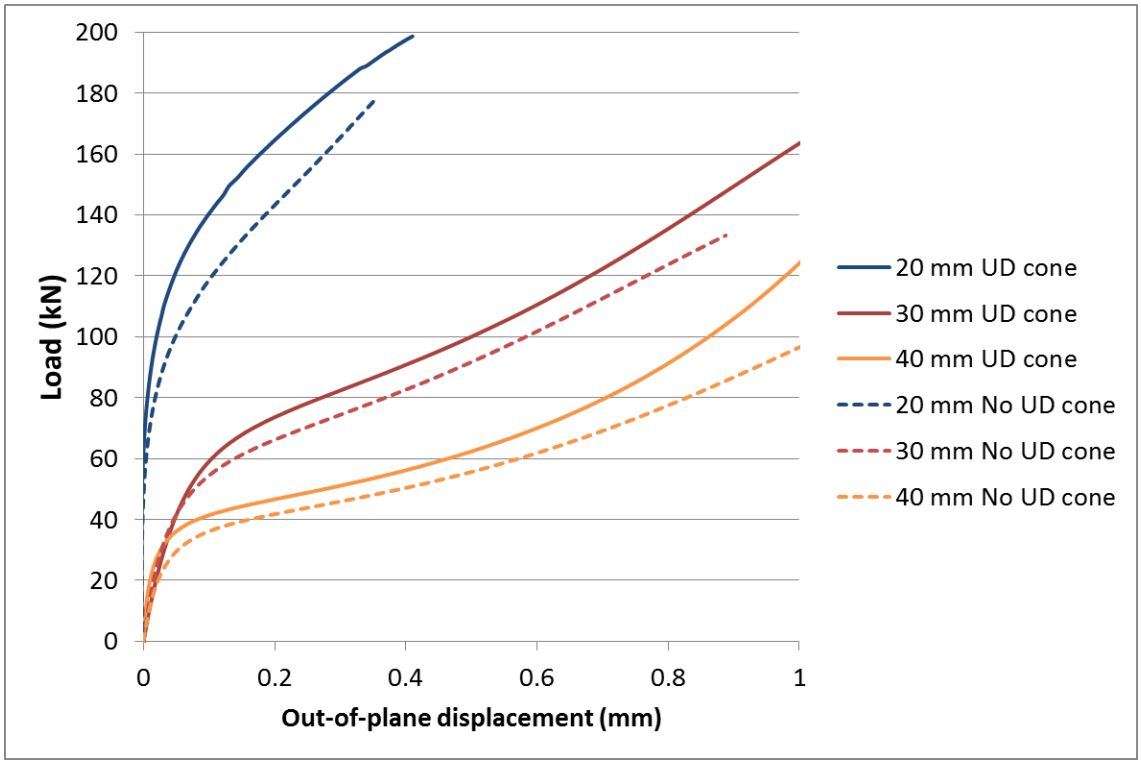

Figure 3: Role of the undamaged cone: a comparison between applied load and corresponding out-of-plane displacement measured at the central node. Plots shown are taken at 20, 30 and 40 mm delamination diameters, with and without the undamaged cone (UC) at 0.1 mm permanent out-of-plane deformation.

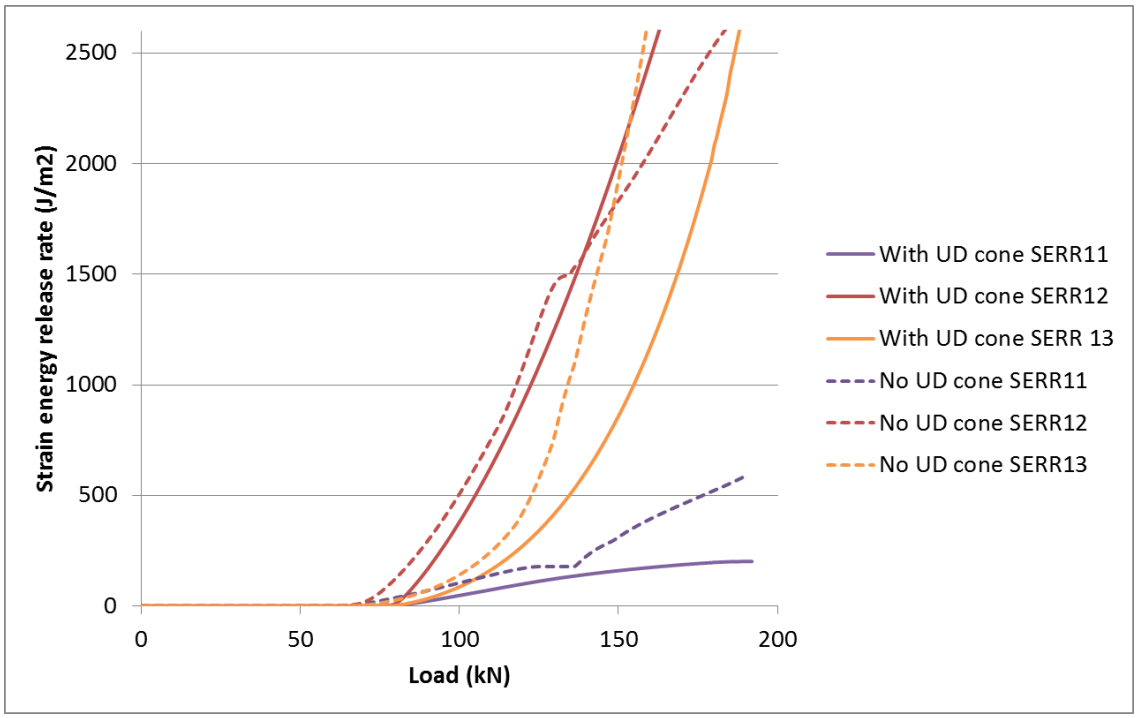

Figure 4: Role of the undamaged cone: a comparison between strain energy release rate and applied load. Plots shown are taken from 30 mm damage diameter with 0.04 mm permanent out-of-plane deformation.

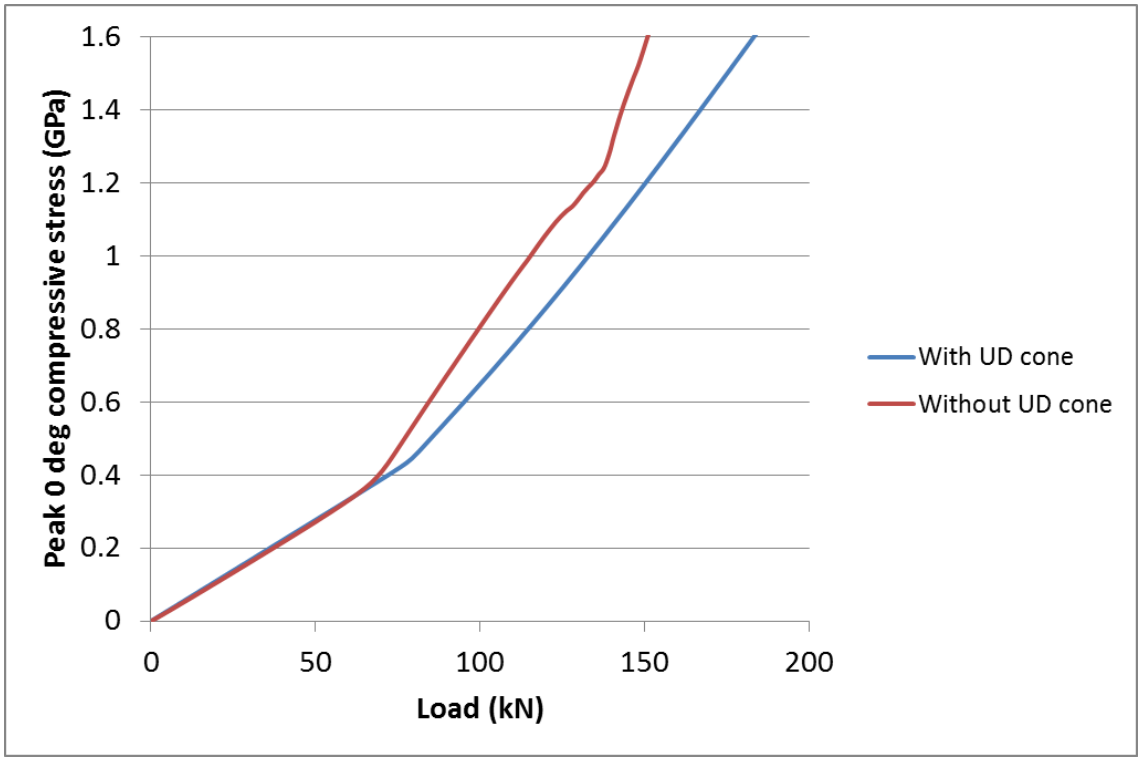

Figure 5: Role of the undamaged cone: a comparison between load and peak 0° compressive stress. Plots shown are taken from 30 mm damage diameter with 0.04 mm permanent out-of-plane deformation.

3.4 Effect of toughness

Delamination growth into the undamaged cone has been observed in some systems prior to the critical loss of load carrying capability. In the plot shown in Fig 6, at 140 kN there is divergence of the load vs. peak compressive stress between the various toughened systems. In this instance, the v-low and low toughened cases exhibited delamination growth into the undamaged cone, increasing the peak compressive stresses exerted at the outer delamination perimeter. The delamination growth into the undamaged cone was caused by the strain energy release rates exceeding the critical value, and is attributed to the local bending stresses occurring in this region. The loss of traction between sublaminates at the undamaged cone subsequently reduced the bending stiffness, leading to a rapid increase out-of-plane displacement and peak compressive stresses. In the medium and high toughness systems, very little damage growth was observed into the undamaged cone, hence a similar response is observed to the infinite toughness case.

The toughness is shown to play a substantial role on the overall failure load. Fig 7 shows the failure loads of systems at 20, 30 and 40 mm diameters across the four toughened systems. It is clear that there is a range of failure loads, varying by ~50%, particularly at 30 and 40 mm delamination diameters. The range of failure loads for a given damage diameter/area is in agreement with previously published experimental work by the authors [16].

The data points circled in fig 7 represents failure governed by the stress exceeding the critical 0° compressive strength, whereas the other regions represent failure occurring through rapid delamination growth. This highlights the competition between failure mechanisms leading to a loss in load carrying capability. Nonetheless, in both instances toughness does play a role in determining failure load, either through supressing delamination growth into the undamaged cone or by suppressing rapid delamination growth at the lateral edges of the delaminated area.

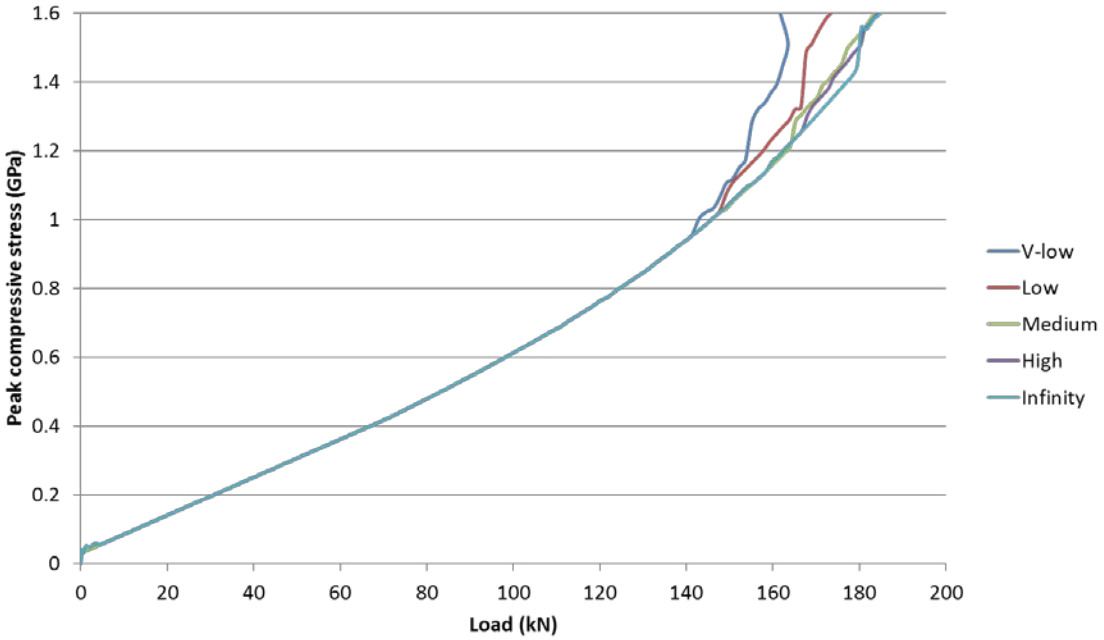

Figure 6: Effect of toughness on load vs. peak compressive stress. Plots shown are taken from 20 mm diameter damage area with 0.02 mm permanent out-of-plane deformation.

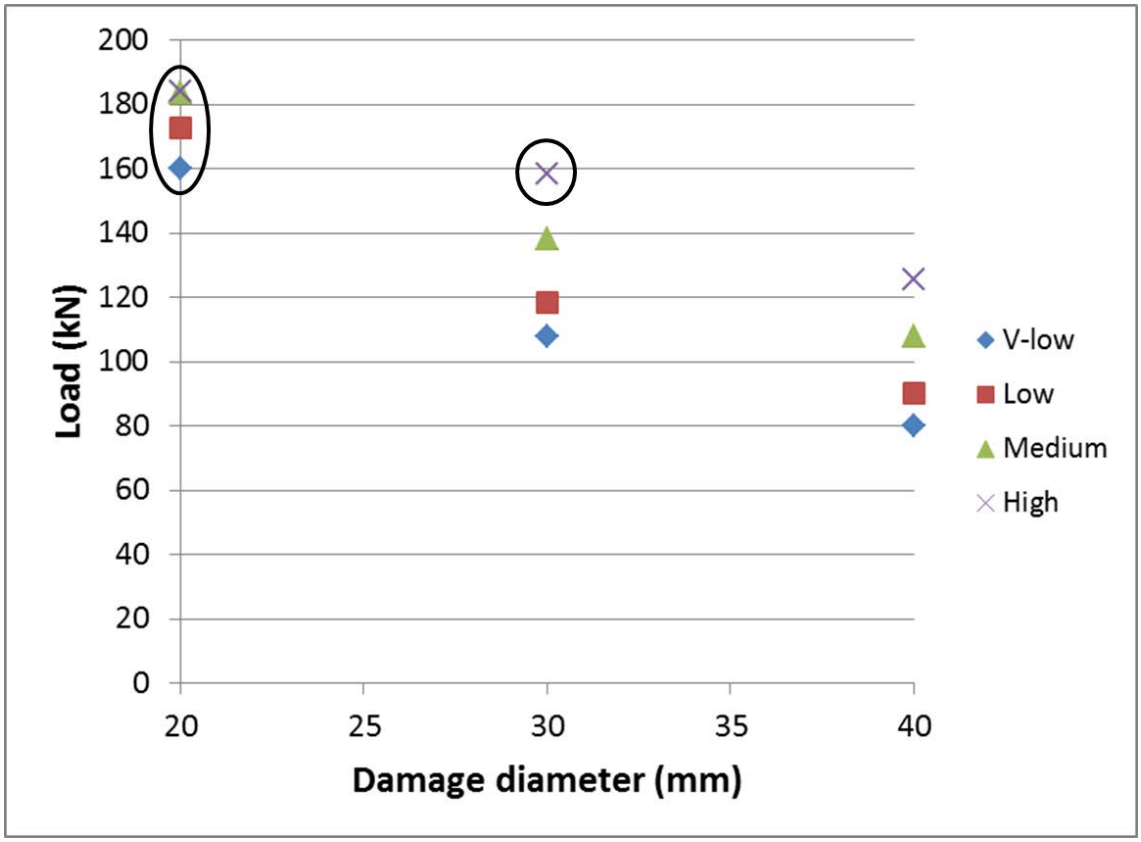

Figure 7: Effect of damage diameters and toughness on failure load. All point in plot taken from 0.1 mm permanent out-of-plane deformation.

3.4 Effect of permanent out-of-plane deformation

The effects of permanent out-of-plane deformation at the impact point were tested against the failure load at 20, 30 and 40 mm damage diameters, see Fig 8. At 20 and 30 mm damage diameters, there is very little difference (< 5%) in failure load across the range of permanent out-of-plane deformation levels. The range of failure loads however is shown to increase to ~25% difference at 40 mm damage diameter where this behaviour is most significant.

Interestingly the systems with the largest permanent out-of-plane deformations exhibited a greater failure load at 40 mm damage diameter. This effect is shown to be associated with the post-buckling response shown in Fig 9. In each of the permanent out-of-plane deformations there is a knee point representing the buckle followed by a rapid increase in out-of-plane deflection in the post-buckle regime. The severity of the knee point and post-buckled response is shown to decrease with an increase in permanent out-of-plane deformation. The ranking order of out-of-plane deflection for a given load is shown to reverse beyond the knee point where the lines are shown to cross over; this is most significant for the 0.1 and 0.4 mm permanent indentations.

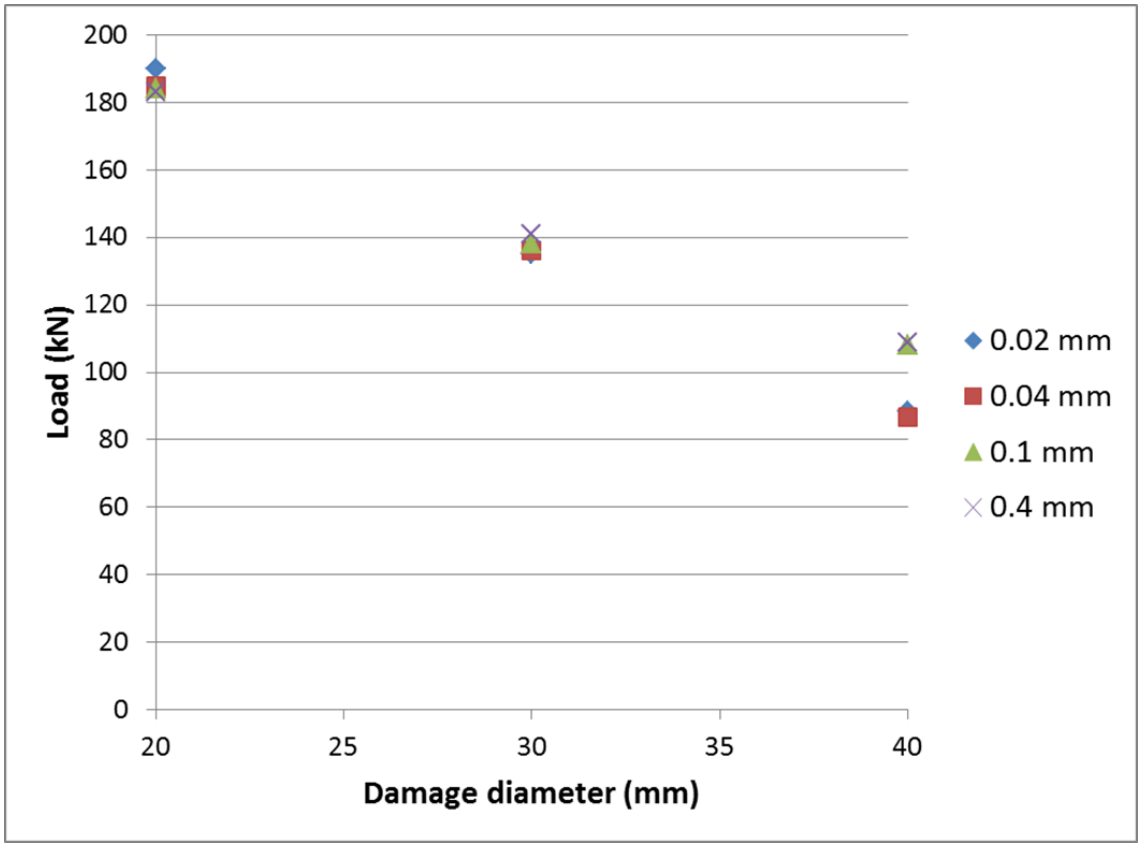

Figure 8: Effect of damage diameters and permanent out-of-plane deformation on failure load. All data points in plot taken from medium toughness system.

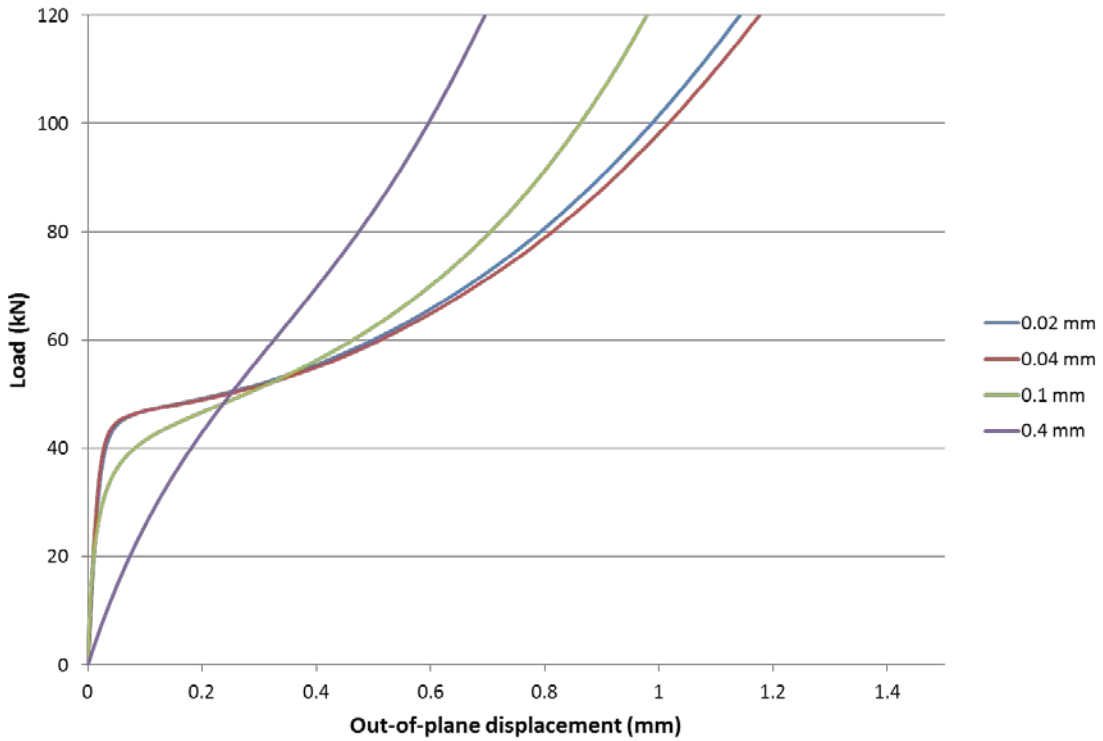

Figure 9: Effect of permanent out-of-plane deformation on load deflection response. All data points in this plot are taken from 40 mm damage diameter models without damage growth.

4 DISCUSSION AND CONCLUSIONS

Beyond damage area, the simulations show that out-of-plane deformation, toughness and the undamaged cone all play a role in determining the residual compressive strength and are important considerations in addition to the size of the damage area. The undamaged cone appears to play an important role by increasing the buckling load and post-buckled response. This in turn reduces the compressive stress and reduces the magnitude of strain energy release rate at the outer edge of the damage area. The work shows that tougher systems offer the greatest benefit to residual strength, a significant ~50% difference to failure load was observed between the v-low and high toughness systems. It is therefore suggested that continued improvements should be made to the mode II and mode III toughness to increase residual CAI strength. This is most important in scenarios where delamination growth into the undamaged cone and rapid delamination growth at the outer edges of the damage area were observed. Regarding the extent of permanent deformation, this parameter was shown to have little effect in comparison to toughness, just ~5% difference to residual strength at 20 and 30 mm damage diameter, but was most significant at 40 mm damage diameter where a difference of ~25% to the failure loads was observed. It is interesting to note that the systems which exhibited the greatest permanent out-of-plane deformations resulted in a greater failure load at 40 mm damage diameter. This is an important observation as toughened systems, as reported in previously published experimental work, typically exhibit a greater extent of permanent out-of-plane deformation associated with local plasticity. This research suggests that toughened systems that are more prone to larger permanent out-of-plane deformations can be used without significant negative consequences to residual CAI load.

ACKNOWLEDGEMENTS

The authors are grateful for the support of Cytec Engineered Materials Ltd., in particular Matthew Jackson the technical point of contact at Cytec. The authors are also appreciative of the EPSRC Knowledge Transfer Secondment scheme which funded this project, grant EP/K503770/1.

REFERENCES

[1] D.D.R. Cartié, P.E. Irving, Effect of resin and fibre properties on impact and compression after impact performance of CFRP. *Composites Part A: Applied Science and Manufacturing*, **33**, 2002, pp. 483-493 (doi:10.1016/S1359-835X(01)00141-5)

[2] D. Delfosse, A. Poursartip, Energy-based approach to impact damage in CFRP laminates. *Compos Part a-Appl S*, **28**, 1997, pp. 647-655 (doi:10.1016/S1359-835X(96)00151-0)

[3] N. Kim, J.D. Achenbach, Quantitative characterization of multiple delaminations in laminated composites using the compton backscatter technique. *J Nondestruct Eval*, **17**, 1998, pp. 53-65 (doi:10.1007/BF02995483)

[4] H.G. Recker, V. Altstadt, W. Eberle, T. Folda, D. Gerth, W. Heckmann, et al., Toughened Thermosets for Damage Tolerant Carbon Fiber Reinforced Composites. *Advanced Materials: the Big Payoff*, 1989, pp. 283-293

[5] L. Reis, M. de Freitas, Damage growth analysis of low velocity impacted composite panels. *Composite structures*, **38**, 1997, pp. 509-515 (doi:10.1016/S0263-8223(97)00086-X)

[6] T.G.D. Rio, R. Zaera, E. Barbero, C. Navarro, Damage in CFRPs due to low velocity impact at low temperature. *Compos Part B-Eng*, **36**, 2005, pp. 41-50 (doi:10.1016/j.compositesb.2004.04.003)

[7] H. Chai, W.G. Knauss, C.D. Babcock, Observation of Damage Growth in Compressively Loaded Laminates. *Experimental Mechanics*, **23**, 1983, pp. 329-337 (doi:10.1007/BF02319260)

[8] H. Yan, C. Oskay, A. Krishnan, L.R. Xu, Compression-after-impact response of woven fiber-reinforced composites. *Composites Science and Technology*, **70**, 2010, pp. 2128-2136 (doi:10.1016/j.compscitech.2010.08.012)

[9] C. Soutis, P.T. Curtis, Prediction of the post-impact compressive strength of CFRP laminated composites. *Composites Science and Technology*, **56**, 1996, pp. 677-684 (doi:10.1016/0266-3538(96)00050-4)

[10] M.R. Wisnom, The role of delamination in failure of fibre-reinforced composites. *Philos T R Soc A*, **370**, 2012, pp. 1850-1870 (doi:10.1098/rsta.2011.0441)

[11] H. Suemasu, W. Sasaki, T. Ishikawa, Y. Aoki, A numerical study on compressive behavior of composite plates with multiple circular delaminations considering delamination propagation. *Composites Science and Technology*, **68**, 2008, pp. 2562-2567 (doi:10.1016/j.compscitech.2008.05.014)

[12] R. Craven, L. Iannucci, R. Olsson, Delamination buckling: A finite element study with realistic delamination shapes, multiple delaminations and fibre fracture cracks. *Compos Part a-Appl S*, **41**, 2010, pp. 684-692 (doi:10.1016/j.compositesa.2010.01.019)

[13] W. Tan, B.G. Falzon, L.N.S. Chiu, M. Price, Predicting low velocity impact damage and Compression-After-Impact (CAI) behaviour of composite laminates. *Compos Part a-Appl S*, **71**, 2015, pp. 212-226 (doi:10.1016/j.compositesa.2015.01.025)

[14] H. Suemasu, W. Sasaki, Y. Aoki, T. Ishikawa, Compressive behavior of impact damaged composite laminates, *In Proc 16th Int Conf on Composite Materials, Kyoto, Japan 8-13 July 2007*, 2007.

[15] R. Olsson, Modelling of impact damage zones in composite laminates for strength after impact. *Aeronaut J*, **116**, 2012, pp. 1349-1365

[16] D.J. Bull, S.M. Spearing, I. Sinclair, Observations of damage development from compression-after-impact experiments using ex situ micro-focus computed

tomography. *Composites Science and Technology*, **97**, 2014, pp. 106-114 (doi:10.1016/j.compscitech.2014.04.008)

[17] M.L. Benzeggagh, M. Kenane, Measurement of mixed-mode delamination fracture toughness of unidirectional glass/epoxy composites with mixed-mode bending apparatus. *Composites Science and Technology*, **56**, 1996, pp. 439-449